Comprehensive Three-Dimensional Analysis of the Neuroretinal Rim in Glaucoma Using High-Density Spectral-Domain Optical Coherence Tomography Volume Scans

Edem Tsikata,[1,2] Ramon Lee,[2] Eric Shieh,[2] Huseyin Simavli,[1–3] Christian J. Que,[1,2] Rong Guo,[4] Ziad Khoueir,[1,2] Johannes de Boer,[5,6] and Teresa C. Chen[1,2]

[1]Department of Ophthalmology, Massachusetts Eye and Ear Infirmary, Boston, Massachusetts, United States
[2]Harvard Medical School, Boston, Massachusetts, United States
[3]Pamukkale Üniversitesi Hastanesi, Denizli, Turkey
[4]Biostatistics, Massachusetts Eye and Ear Infirmary, Boston, Massachusetts, United States
[5]LaserLaB Amsterdam, Department of Physics and Astronomy, Vrije Universiteit, Amsterdam, The Netherlands
[6]Department of Ophthalmology, Vrije Universiteit Medical Center, Amsterdam, The Netherlands

Correspondence: Teresa C. Chen, Massachusetts Eye and Ear Infirmary, Glaucoma Service, 243 Charles Street, Boston, MA 02114, USA; teresa_chen@meei.harvard.edu.

Submitted: April 24, 2016
Accepted: August 8, 2016

Citation: Tsikata E, Lee R, Shieh E, et al. Comprehensive three-dimensional analysis of the neuroretinal rim in glaucoma using high-density spectral-domain optical coherence tomography volume scans. *Invest Ophthalmol Vis Sci*. 2016;57:5498–5508. DOI:10.1167/iovs.16-19802

Purpose. To describe spectral-domain optical coherence tomography (OCT) methods for quantifying neuroretinal rim tissue in glaucoma and to compare these methods to the traditional retinal nerve fiber layer thickness diagnostic parameter.

Methods. Neuroretinal rim parameters derived from three-dimensional (3D) volume scans were compared with the two-dimensional (2D) Spectralis retinal nerve fiber layer (RNFL) thickness scans for diagnostic capability. This study analyzed one eye per patient of 104 glaucoma patients and 58 healthy subjects. The shortest distances between the cup surface and the OCT-based disc margin were automatically calculated to determine the thickness and area of the minimum distance band (MDB) neuroretinal rim parameter. Traditional 150-μm reference surface–based rim parameters (volume, area, and thickness) were also calculated. The diagnostic capabilities of these five parameters were compared with RNFL thickness using the area under the receiver operating characteristic (AUROC) curves.

Results. The MDB thickness had significantly higher diagnostic capability than the RNFL thickness in the nasal (0.913 vs. 0.818, $P = 0.004$) and temporal (0.922 vs. 0.858, $P = 0.026$) quadrants and the inferonasal (0.950 vs. 0.897, $P = 0.011$) and superonasal (0.933 vs. 0.868, $P = 0.012$) sectors. The MDB area and the three neuroretinal rim parameters based on the 150-μm reference surface had diagnostic capabilities similar to RNFL thickness.

Conclusions. The 3D MDB thickness had a high diagnostic capability for glaucoma and may be of significant clinical utility. It had higher diagnostic capability than the RNFL thickness in the nasal and temporal quadrants and the inferonasal and superonasal sectors.

Keywords: glaucoma, spectral-domain optical coherence tomography, optic disc, optic nerve, neuroretinal rim

Glaucoma is the world's leading cause of permanent blindness and is a progressive neurodegenerative disease characterized by irreversible loss of retinal ganglion cells.[1] Death of retinal ganglion cells produces structural changes that include thinning of the retinal nerve fiber layer (RNFL), macular ganglion cell layer, and neuroretinal rim tissue.[2–4] These structural changes can be objectively quantified with spectral-domain (SD) optical coherence tomography (OCT), which is used to help diagnose glaucoma and monitor disease progression. In particular, the circumpapillary RNFL thickness scan is the most commonly used OCT parameter to quantify structural change in glaucoma. The RNFL parameter, however, is limited by a high rate of artifacts, partly due to the difficulty in segmenting the RNFL, which decreases in reflectivity with glaucoma.[5] The two-dimensional (2D) RNFL parameter also does not fully use the three-dimensional (3D) imaging capabilities of SD-OCT. Newer SD-OCT glaucoma parameters derived from high-density 3D volume datasets may potentially improve on the traditional 2D RNFL thickness parameter by addressing both issues and enhancing diagnostic sensitivity. Because of the increased acquisition speeds of SD-OCT compared with time-domain OCT, high-density 3D volume datasets depicting true optic nerve topography are now possible, without the need for realignment of A-lines within a single frame.[6]

The minimum distance band (MDB) is a 3D SD-OCT neuroretinal rim parameter that offers potential advantages over the traditional 2D RNFL thickness parameter.[7,8] It objectively quantifies neuroretinal rim tissue using the anatomically accurate position of the disc margin, as determined from OCT data. The parameter is delimited by structures (the internal limiting membrane [ILM] and the retinal pigment epithelium/Bruch's membrane complex [RPE/BM])[9] whose visibilities are not significantly modified by glaucoma.[10] In theory, the MDB may be more robust than the RNFL thickness,

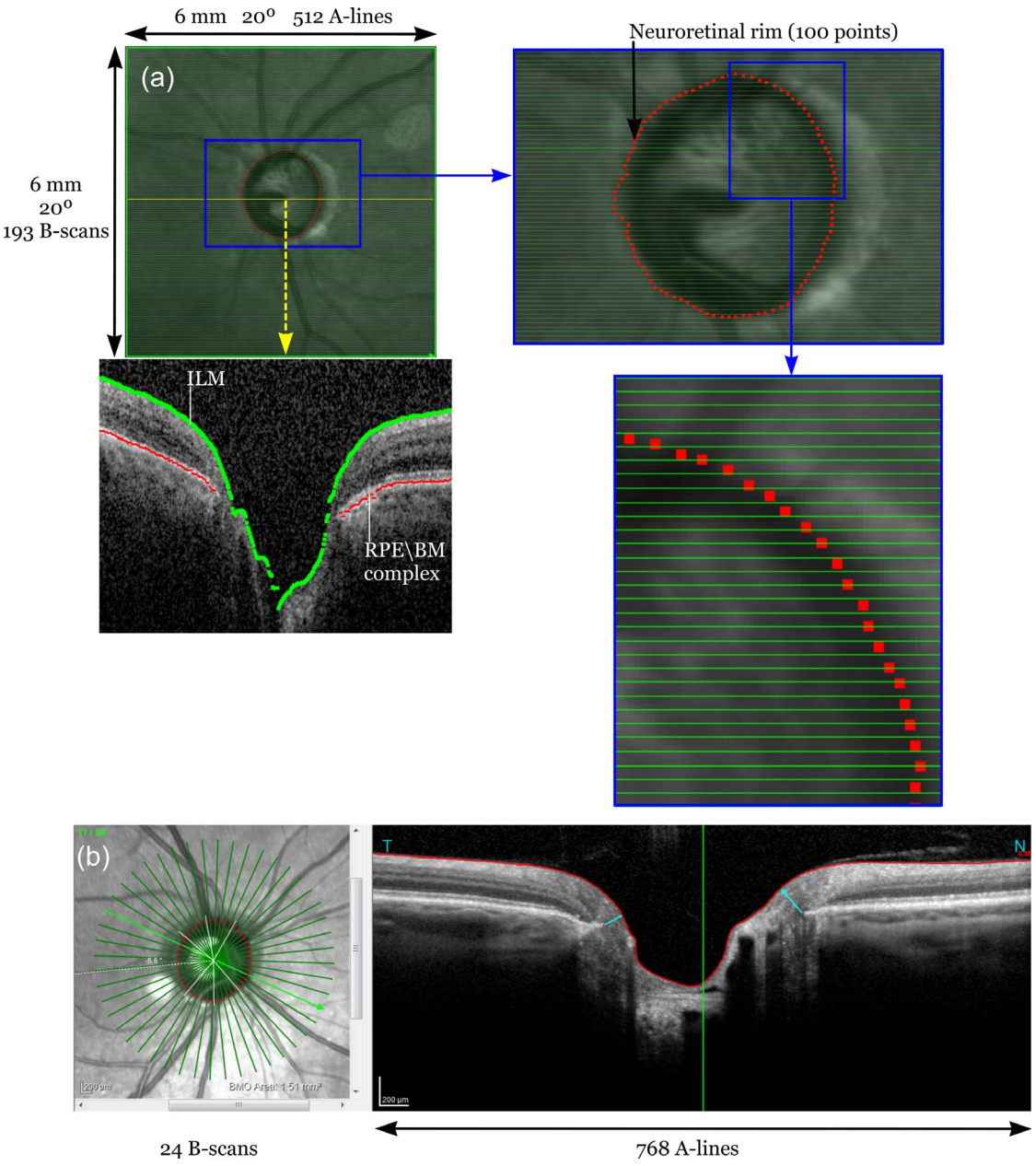

Figure 1. The MDB volumetric high-density raster scan protocol compared with the BMO-MRW radial scan protocol. In (**a**), the *horizontal green lines* represent the 193 raster lines, which are used to reconstruct the OCT disc margin (*100 red points*), defined as the RPE\BM border. The *lower left image* in (**a**) is an OCT B-scan at the position of the *yellow line*. It depicts the automated segmentation of the ILM and the RPE\BM complex. In (**b**), the 24 radial scan pattern of the BMO-MRW protocol is shown. The OCT disc margin is reconstructed at 48 positions (*48 red points*) and is defined as the BMO border.

because it is derived from dense volumetric data, whereas the RNFL thickness is derived from a single B-scan. The MDB also differs from current OCT optic nerve software parameters (e.g., rim volume, rim area, and rim thickness), in that it is not defined by an arbitrary reference surface above the RPE. Optic nerve head measurements are also available on the Cirrus instrument (Carl Zeiss Meditec, Dublin, CA, USA),[11] but the volumetric protocol (200 A-lines in 200 B-scans) is less densely sampled than the one in this study, which not only uses 512 A-lines in the 193 B-scans but also averages the 193 raster scans (Fig. 1a).[12]

Since initial descriptions of this 3D neuroretinal rim parameter, a similar parameter called the Bruch's Membrane Opening–Minimum Rim Width (BMO-MRW) has been investigated on the Spectralis platform (Heidelberg Engineering, Heidelberg, Germany). The BMO-MRW uses scans of 24 radial lines over the optic nerve head (Fig. 1b).[13] He et al.[14] suggested that this parameter may be the most sensitive OCT parameter for detecting glaucoma progression in the primate glaucoma model. Human studies using this BMO-MRW parameter also have suggested that this parameter has higher diagnostic capability than the 2D RNFL thickness measurement, but it is unclear whether this improvement is significantly better.[13]

The MDB defines the OCT-based disc margin as the termination of the RPE/BM complex, whereas in the BMO-MRW, the BM opening is identified as the disc margin. Strouthidis et al.[15] and Drexler and Fujimoto[16] state that it is uncertain whether the BM in isolation can be resolved by SD-

OCT. The termination of the RPE/BM complex may thus more consistently describe the disc margin visible in SD-OCT images.

This article presents a framework for calculating the MDB neuroretinal rim thickness and area from high-density 3D raster scans across the optic nerve head on the Spectralis SD-OCT platform. It also compares the MDB with the traditional 2D RNFL parameter and with existing neuroretinal rim parameters that are based on the 150-μm reference surface.

Materials and Methods

The subjects were recruited as a part of the ongoing Massachusetts Eye and Ear Infirmary 5-year prospective Spectral-Domain Optical Coherence Tomography in Glaucoma Study. These patients were a cross-sectional sampling of patients recruited between September 2009 and July 2014. The study had institutional review board approval. Research was conducted in accordance with the tenets of the declaration of Helsinki and the regulations of the Health Insurance Portability and Accountability Act. One eye per subject, selected randomly, was analyzed. All participants underwent a comprehensive ocular examination by a glaucoma specialist (TCC) that included history, visual acuity, refraction, Goldmann applanation tonometry, slit-lamp biomicroscopy, gonioscopy, dilated ophthalmoscopy, ultrasound pachymetry, stereophotography (Visucam Pro NM; Carl Zeiss Meditec), and visual field testing (Swedish Interactive Threshold Algorithm 24–2 test of the Humphrey visual field analyzer 750i; Carl Zeiss Meditec).

Patients were eligible to participate in the study if they consented to OCT imaging on the same day as their full eye examination, disc photography, and visual field testing. Inclusion and exclusion criteria were similar to those used in past studies.[2,17–22] Patients were included if they had a spherical equivalent between −5 and +5 diopters and a best-corrected visual acuity of 20/40 or better. These patients also required reliable visual fields, defined as fixation losses ≤33%, false positives ≤20%, and false negatives ≤20%. Patients were excluded if they had congenital abnormalities of the anterior chamber, corneal scarring or opacity, diabetic retinopathy, visual field loss due to a nonglaucoma condition, or a dilated pupil diameter less than 2 mm.

Healthy subjects had no ocular disease except for mild cataracts and had a normal Glaucoma Hemifield Test. The asymmetry of their cup-to-disc ratio measurements was less than 0.2.

Glaucoma patients were diagnosed by characteristic changes of the optic nerve with corresponding abnormal visual fields. Visual fields were considered abnormal if three or more contiguous test locations in the pattern SD plot were depressed by 5 dB or more or if two contiguous test locations showed defects with one location depressed by 5 dB or more and the other by 10 dB or more.

Volumetric Imaging of the Optic Nerve Head

Volumetric scans were acquired on the Spectralis OCT instrument (Spectralis software version 5.4.8.0; Heidelberg Engineering). The OCT protocol consisted of 193 B-scans centered on the optic nerve head. The field of view was 20 × 20 degrees, corresponding to a square region approximately 6 × 6 mm. Automatic real-time tracking functionality was enabled, and three frames at each scanning location were acquired and averaged to create the final OCT B-scans. The Heidelberg quality score was used as a proxy for the volumetric scan quality, and all included subjects had an RNFL scan quality of 15 or higher on a scale ranging from 0 to 40.

To evaluate the reproducibility of the MDB thickness, the eyes of 50 subjects were scanned twice within the same day. Bland-Altman analysis was performed on the MDB measurements derived from the two datasets to determine the intertest variability.

Image Analysis of SD-OCT High-Density Volume Scans

To calculate the five neuroretinal rim parameters, the ILM and the RPE/BM complex[8] were automatically segmented in each image (Fig. 2). Image analysis was performed with C++ software using the open source libraries Insight Segmentation and Registration Toolkit (ITK version 4.3, Insight Software Consortium; Kitware, Inc., Clifton Park, NY, USA) and Open Source Computer Vision (OpenCV version 2.4.3; Willow Garage, Menlo Park, CA, USA).

To segment the ILM, images were denoised with a 5-pixel median filter, and a Canny edge detector[23] was used to find the contour representing the ILM.

The disc margin was detected by reconstructing the RPE/BM complex from the individual B-scans. Identification of the disc margin required calculation of the RPE/BM terminations where this structure was discontinuous, and delineation of the unbroken structure in regions where it was continuous. A three-level Otsu[24] filter was used to locate the highly reflective pixels of the RPE, and a Canny edge detector was used to delineate borders of the RPE/BM complex. Bruch's membrane was not consistently visible as a structure distinct from the RPE.

The MDB (Fig. 3) was calculated by building a 3D model of the RPE/BM complex. The central axis of the disc was determined by finding the centroid of the opening in the RPE/BM. For each angular interval of 3.6 degrees (for calculation of the MDB thickness at 100 points around the rim), the point on the disc margin closest to the disc axis was identified, and the shortest distance from this point to the ILM was calculated. From the distance measurements, the MDB thickness values for the global, quadrant, and sector regions were determined.

The area of the MDB (Fig. 3) was calculated by subdividing the band into a series of quadrilaterals. The vertices of the quadrilaterals were two adjacent points on the disc margin (R1, R2) and their corresponding closest points on the ILM (I1, I2). The areas of the two triangles formed by the four points were calculated using Heron's formula. This process was repeated around the disc margin, and the results were summed to give the global, quadrant, and sector area measurements. This technique differs from the procedure of Gardiner et al.,[25] in which a set of trapezoids was used to calculate the neuroretinal rim area. In this study's method, the two rim points and two ILM points were not constrained to lie in the same plane.

A reference surface 150 μm above the RPE has been used to determine optic nerve parameters for both commercially available time-domain OCT and SD-OCT machines.[26] We determined neuroretinal rim volume, rim area, and rim thickness using a 150-μm reference surface. Figure 4a illustrates the results of neuroretinal rim tissue volume calculations. The neuroretinal rim was bounded above by the ILM, below by the 150-μm reference surface, and radially by the optic disc border. The neuroretinal rim area (Fig. 4b) was determined by finding the projection of the rim tissue on the transverse plane. The rim thickness was calculated by dividing the rim volume by the rim area.

Statistical Analysis

Statistical analysis was performed using SAS (SAS Institute, Inc., Cary, NC, USA). The demographic and ocular characteristics of

Investigative Ophthalmology & Visual Science

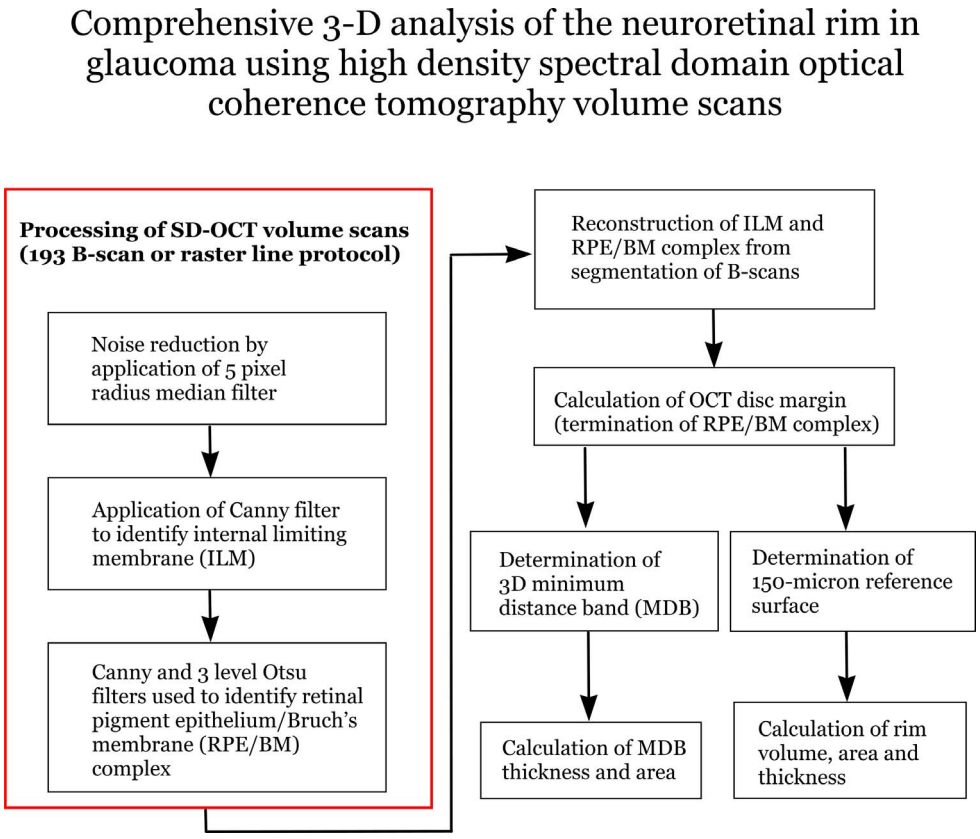

Figure 2. A flowchart summarizing the steps involved to calculate five neuroretinal rim parameters from 3D SD-OCT (Spectralis; Heidelberg Engineering) high-density volume scans. The five neuroretinal rim parameters include the MDB thickness, MDB area, rim volume, rim area, and rim thickness.

the normal and glaucoma groups were compared with χ^2 tests for categorical variables and nonpaired 2-tailed Student's *t*-tests for continuous variables (Table 1). Significance was established if the *P* values were less than 0.05. The areas under the receiver operating characteristic (AUROC) curves were compared using the method of Delong et al.[27]

Results

Table 1 describes the clinical characteristics of the 162 eyes of 162 subjects in the study population. There were 58 healthy subjects and 104 glaucoma patients in this study. The datasets of 10 eligible patients were excluded due to acquisition and segmentation artifacts. The proportion of Caucasian subjects in the healthy and glaucoma groups was nearly equal (65.4% vs. 65.5%). The combined proportions of the African American and Hispanic subjects (27.0% and 25.9%) were also closely balanced between the two groups (Table 1).

Table 2 shows that the mean values of the RNFL thickness and the five neuroretinal rim parameters for the healthy and glaucoma groups are significantly reduced in glaucoma patients compared with healthy subjects for all regions (global,

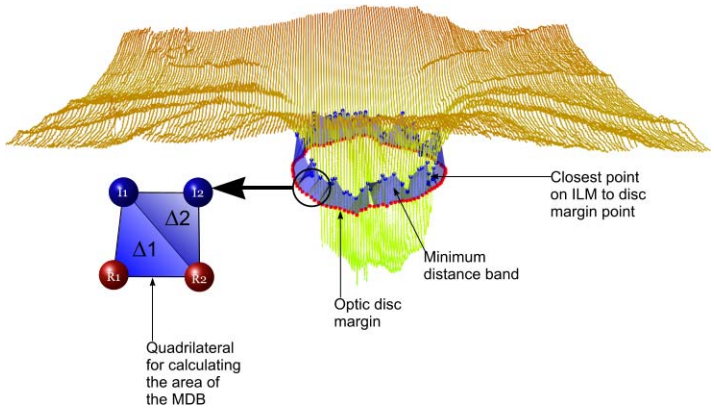

Figure 3. Diagram showing the MDB neuroretinal rim parameter. The MDB thickness is measured by finding the closest distances from points on the disc margin (*red points*) to the ILM or cup surface (*blue points*). The MDB area is calculated by summing the areas of triangles formed by disc margin points (R1 and R2) and points (I1 and I2) on the ILM, which may not be coplanar. This example is the left eye of a 67-year-old African American man with primary open-angle glaucoma. His visual field mean deviation is –16.6 dB.

Investigative Ophthalmology & Visual Science

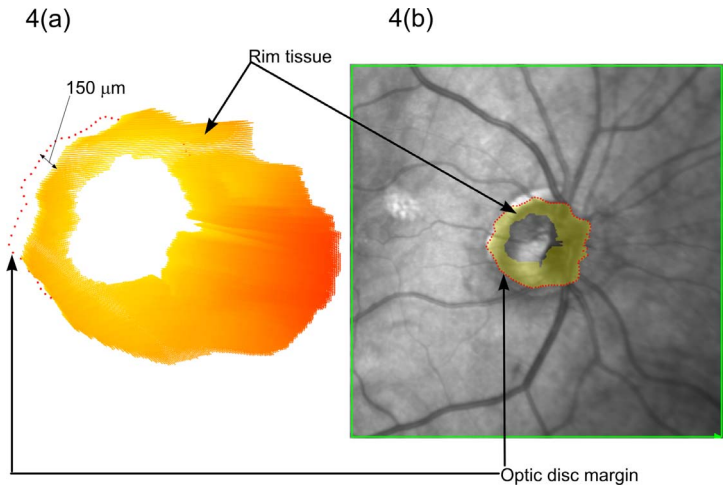

Figure 4. Calculation of neuroretinal rim volume and area from SD-OCT volume scans using a reference surface 150 μm above the OCT disc margin. (**a**) The neuroretinal rim tissue (shown in *yellow*) is calculated for the right eye of a healthy subject. The OCT-based disc margin or RPE/BM complex is shown by *red points*. The neuroretinal rim was bounded above by the ILM, below by the 150-μm reference surface, and radially by the optic disc border. (**b**) The projection of the rim tissue and disc margin on an infrared fundus photo. The OCT-based disc margin (*red points*) shows good correspondence with the disc border on the fundus photo.

all quadrants, and all four sectors; P values < 0.001). The receiver operating characteristic (ROC) curves for the global measurements of the six parameters (Fig. 5) showed that the global measurements had statistically similar diagnostic capability ($P > 0.05$).

In Table 3, the diagnostic capabilities of the five neuroretinal rim parameters are compared with the RNFL thickness parameter using pairwise comparisons of the AUROC curves for the global, quadrant, and sector regions. Table 3 shows that the diagnostic capability of the 3D MDB neuroretinal rim thickness was higher than that of 2D RNFL thickness in the nasal (0.913 vs. 0.818, $P = 0.004$; Fig. 6) and temporal (0.922 vs. 0.858, $P = 0.026$; Fig. 7) quadrants and superonasal (0.933 vs. 0.868, $P = 0.012$) and inferonasal (0.950 vs. 0.897, $P = 0.011$) sectors. The other parameters (MDB area, neuroretinal rim volume, area, and thickness) were comparable to the RNFL thickness in diagnostic capability. The inferior MDB thickness quadrant had the highest AUROC of the quadrants (0.966), and the inferotemporal sector had the highest AUROC for all quadrants and sectors (0.968). The highest MDB thickness AUROC values (0.968) were associated with global and inferotemporal MDB thickness. The MDB thickness had a significantly higher AUROC than the rim volume in only the global (0.968 vs. 0.952, $P = 0.030$) and the superonasal (0.933 vs. 0.909, $P = 0.015$) regions (data not shown in the final figures and tables).

Table 3 also shows that there were no statistically significant differences between AUROC values for MDB area and RNFL thickness in any region ($P = 0.055$–0.827). The global MDB area had the highest AUROC at 0.969, followed by the inferotemporal sector at 0.955 and the inferior quadrant at 0.952. The MDB area also had significantly higher AUROC values than the rim area in all fields except the nasal quadrant (0.886 vs. 0.841, $P = 0.104$) and the superonasal sector (0.886 vs. 0.852, $P = 0.173$) (data not shown in the final figures and tables).

The rim volume parameter (0.895–0.952) had similar diagnostic capability to the RNFL thickness. There were no statistically significant differences in diagnostic capability ($P = 0.084$–0.912) except for the nasal rim volume (0.895 vs. 0.818, $P = 0.025$), which had a higher AUROC than the nasal RNFL thickness. The highest AUROC for the rim volume was for the global field at 0.952, followed by the inferior quadrant at 0.950 and the inferotemporal sector at 0.949.

The rim area (0.841–0.908) had lower diagnostic capability than the RNFL thickness in the global (0.908 vs. 0.954, $P = 0.029$), inferior (0.897 vs. 0.958, $P = 0.005$), and inferotemporal (0.894 vs. 0.958, $P = 0.006$) zones. The highest AUROC was for global rim area at 0.908, followed by the inferior (0.897) and inferotemporal regions (0.894).

Lastly, the rim thickness (0.878–0.952) had similar diagnostic capability ($P = 0.096$–0.973) compared with RNFL thickness for all regions. The diagnostic capability of the rim thickness lay between the capabilities of the rim volume and area, with the rim volume generally having the highest AUROC values of the three reference surface dependent parameters. The highest rim thickness AUROC value was for inferior rim thickness at 0.952, followed by global rim thickness at 0.944, and then the inferotemporal rim thickness at 0.943.

In the 162 volumetric scans, an average of 11 frames of 193, or 5.7%, had an artifact.

Table 1. Clinical Characteristics of the Normal and Open Angle Glaucoma Study Populations

Characteristic	Normal	Glaucoma	P^*
Number of eyes	58	104	
Number of right eyes/ left eyes	32/26	52/52	0.528
Mean age, y	54.34 ± 15.52	67.96 ± 11.99	<0.0001
Spherical equivalent, diopters	−0.40 ± 1.80	−0.65 ± 1.83	0.418
VF			
Mean deviation, dB	−1.42 ± 1.93	−11.85 ± 7.61	<0.0001
Pattern SD	1.52 ± 0.29	8.34 ± 3.21	<0.0001
Race, *n* (%)			
Caucasian	38 (65.5)	68 (65.4)	
African American	8 (13.8)	22 (21.2)	
Hispanic	7 (12.1)	6 (5.8)	
Asian	5 (8.6)	4 (3.8)	
Other	0 (0)	4 (3.8)	

Results are expressed as the mean ± SD unless otherwise indicated.

* Healthy versus glaucoma.

Table 2. The Mean Values of SD-OCT Diagnostic Parameters Are Shown for Healthy and Glaucoma Patients

Diagnostic Parameter and Region	Mean ± SD		*P*, Healthy vs. Glaucoma
	Normal	Glaucoma	
RNFL thickness, μm			
Global	94.53 ± 12.24	58.67 ± 15.41	<0.001
Inferior	122.7 ± 20.19	64.16 ± 23.21	<0.001
Superior	114.1 ± 20.20	69.69 ± 20.35	<0.001
Nasal	70.97 ± 13.89	50.69 ± 18.21	<0.001
Temporal	69.88 ± 13.95	49.84 ± 16.55	<0.001
IT	138.0 ± 23.83	64.89 ± 29.76	<0.001
IN	107.6 ± 27.35	63.45 ± 23.51	<0.001
ST	128.8 ± 23.64	74.94 ± 26.23	<0.001
SN	99.43 ± 22.68	64.39 ± 21.61	<0.001
MDB thickness, mm			
Global	0.312 ± 0.041	0.176 ± 0.053	<0.001
Inferior	0.349 ± 0.049	0.174 ± 0.065	<0.001
Superior	0.344 ± 0.059	0.188 ± 0.067	<0.001
Nasal	0.312 ± 0.049	0.192 ± 0.068	<0.001
Temporal	0.245 ± 0.041	0.152 ± 0.049	<0.001
IT	0.338 ± 0.051	0.148 ± 0.069	<0.001
IN	0.359 ± 0.056	0.200 ± 0.071	<0.001
ST	0.345 ± 0.057	0.180 ± 0.071	<0.001
SN	0.351 ± 0.062	0.203 ± 0.072	<0.001
MDB area, mm^2			
Global	2.088 ± 0.362	1.064 ± 0.371	<0.001
Inferior	0.584 ± 0.118	0.262 ± 0.125	<0.001
Superior	0.608 ± 0.156	0.288 ± 0.126	<0.001
Nasal	0.526 ± 0.133	0.298 ± 0.130	<0.001
Temporal	0.371 ± 0.105	0.215 ± 0.087	<0.001
IT	0.282 ± 0.075	0.106 ± 0.060	<0.001
IN	0.309 ± 0.067	0.157 ± 0.075	<0.001
ST	0.301 ± 0.086	0.129 ± 0.068	<0.001
SN	0.307 ± 0.099	0.159 ± 0.075	<0.001
Rim volume, mm^3			
Global	0.2585 ± 0.1088	0.0661 ± 0.0609	<0.001
Inferior	0.0917 ± 0.0388	0.0203 ± 0.0235	<0.001
Superior	0.0734 ± 0.0369	0.0183 ± 0.0191	<0.001
Nasal	0.0648 ± 0.0340	0.0201 ± 0.0216	<0.001
Temporal	0.0287 ± 0.0189	0.0075 ± 0.0089	<0.001
IT	0.0419 ± 0.0200	0.0073 ± 0.0125	<0.001
IN	0.0498 ± 0.0240	0.0130 ± 0.0137	<0.001
ST	0.0344 ± 0.0194	0.0074 ± 0.0094	<0.001
SN	0.0390 ± 0.0199	0.0109 ± 0.0114	<0.001
Rim area, mm^2			
Global	1.555 ± 0.345	0.785 ± 0.428	<0.001
Inferior	0.457 ± 0.110	0.211 ± 0.146	<0.001
Superior	0.427 ± 0.118	0.215 ± 0.140	<0.001
Nasal	0.402 ± 0.096	0.232 ± 0.135	<0.001
Temporal	0.269 ± 0.118	0.128 ± 0.102	<0.001
IT	0.221 ± 0.061	0.086 ± 0.081	<0.001
IN	0.236 ± 0.065	0.124 ± 0.076	<0.001
ST	0.206 ± 0.064	0.094 ± 0.076	<0.001
SN	0.221 ± 0.064	0.121 ± 0.075	<0.001
Rim thickness, mm			
Global	0.162 ± 0.042	0.074 ± 0.037	<0.001
Inferior	0.197 ± 0.053	0.079 ± 0.045	<0.001
Superior	0.168 ± 0.061	0.071 ± 0.045	<0.001
Nasal	0.158 ± 0.064	0.072 ± 0.048	<0.001
Temporal	0.100 ± 0.029	0.050 ± 0.030	<0.001
IT	0.187 ± 0.052	0.066 ± 0.048	<0.001
IN	0.207 ± 0.065	0.086 ± 0.049	<0.001
ST	0.162 ± 0.057	0.061 ± 0.045	<0.001
SN	0.172 ± 0.073	0.075 ± 0.049	<0.001

Values are shown for RNFL thickness and five neuroretinal rim parameters: MDB thickness, MDB area, rim volume, rim area, and rim thickness. IN, inferonasal; IT, inferotemporal; SN, superonasal; ST, superotemporal.

The reproducibility of the MDB program was evaluated using scans of 76 eyes from 50 subjects (20 healthy subjects, 16 glaucoma patients, and 14 subjects with other conditions). The intertest variability was calculated by dividing the difference in the measurements by their average, and a Bland-Altman diagram was created (Fig. 8). The mean of the intertest variability was 0.84%, and its SD was 5.18%.

The MDB thickness showed a significant correlation ($P = 0.032$) with age, with a slope of –0.75 μm per year. Therefore, the mean expected reduction in the global MDB thickness due to the glaucoma group being 13.6 years older than the healthy cohort is 10.2 μm (or –0.75 μm × 13.6 years), which is smaller than the measured difference between the normal and glaucoma groups of 136 μm.

Discussion

Neuroretinal rim parameters, like the proposed MDB[7] thickness and area and later variations, such as the BMO-MRW,[13] are of clinical interest because they are uniquely designed to quantify neuroretinal rim tissue from 3D SD-OCT images and because they do not use a reference surface for calculations. Older time-domain OCT diagnostic techniques still remain in SD-OCT machines. These methods include peripapillary RNFL thickness and neuroretinal rim parameters (i.e., rim volume, area, and thickness) which are derived from a flat reference plane 150 or 200 μm above a curved RPE surface. In contrast to time-domain OCT methods, which use a flat reference plane, newer SD-OCT diagnostic parameters do not need a reference surface[9] but instead use OCT-based landmarks, such as the RPE/BM complex, to more accurately determine a neuroretinal rim border.[6,13] This work establishes that the reconstruction of the ILM and RPE/BM complex from high-density raster scans can be used to generate multiple 3D parameters with high diagnostic capabilities for glaucoma, the most promising being the MDB thickness.

This study demonstrates that the MDB thickness has significantly higher ($P = 0.004$–0.026) diagnostic capability compared with 2D RNFL thickness measurements in the nasal, temporal, inferonasal, and superonasal fields. Both the 2D RNFL thickness parameter and the 3D MDB parameters quantify the cross-sectional band through which nerve tissue travels as it exits the eye going toward the brain, and the parameters are sensitive to neuronal loss. However, because the MDB comprises a higher percentage of nerve tissue than the RNFL thickness, the MDB may be a better surrogate measure of nerve tissue than RNFL thickness. The surface nerve fiber layer of the optic nerve head, of which the MDB is a cross-section, consists of approximately 94% neurons and 5% astrocytes.[28] In contrast, SD-OCT studies have suggested that 48.8% to 65.1% of the total RNFL thickness may be glial and vascular tissue, and this large "floor effect" of glial tissue and blood vessels varies from machine to machine (RNFL thickness

Investigative Ophthalmology & Visual Science

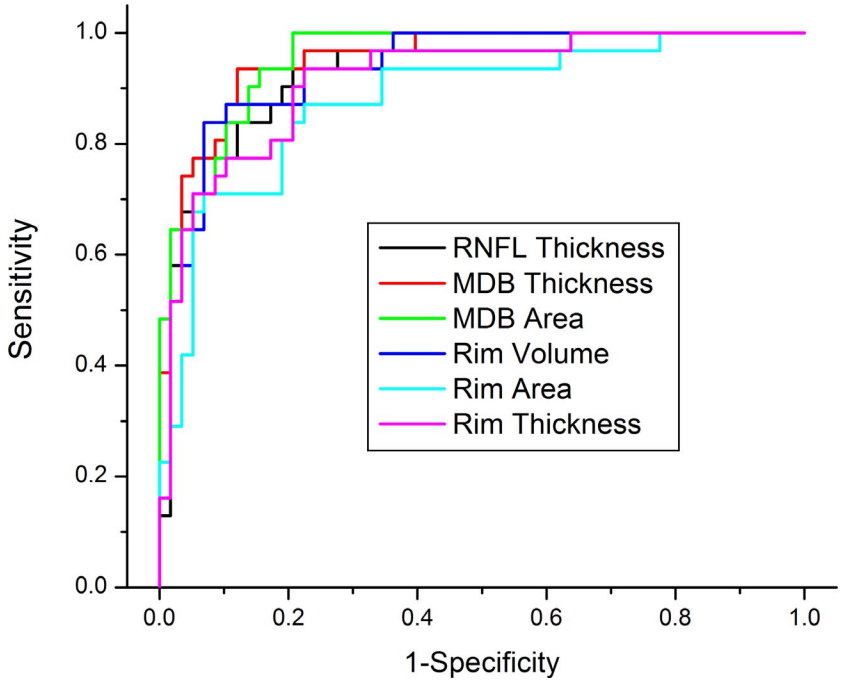

Figure 5. The ROC curve of the global RNFL thickness (AUROC = 0.954), MDB thickness (AUROC 0.968), MDB area (AUROC 0.969), rim volume (AUROC 0.952), rim area (AUROC 0.908), and rim thickness (AUROC 0.944).

floor measurement: Spectralis, 49.2 μm; Cirrus, 57.0 μm; RTVue [Optovue, Fremont, CA, USA], 64.7 μm).[29]

The BMO-MRW (Spectralis Glaucoma Module Premium Edition; Heidelberg Engineering), a parameter similar to the MDB neuroretinal rim thickness, has been studied by several authors,[13,30–34] but it is unclear if the BMO-MRW has significantly higher diagnostic ability than the RNFL thickness. Initial studies of the diagnostic capability of this parameter involved manual identification of the BMO and the ILM.[13] In contrast to the 193 raster line volume scan from which the MDB neuroretinal rim parameter is obtained (Fig. 1a), the BMO-MRW is derived from 24 radial line scans over the optic nerve (Fig. 1b). Chauhan et al.[13] suggested that the BMO-MRW may have enhanced diagnostic capability compared with the RNFL thickness (AUROC of 0.96 for global BMO-MRW compared with 0.92 for RNFL thickness). The ROC curves

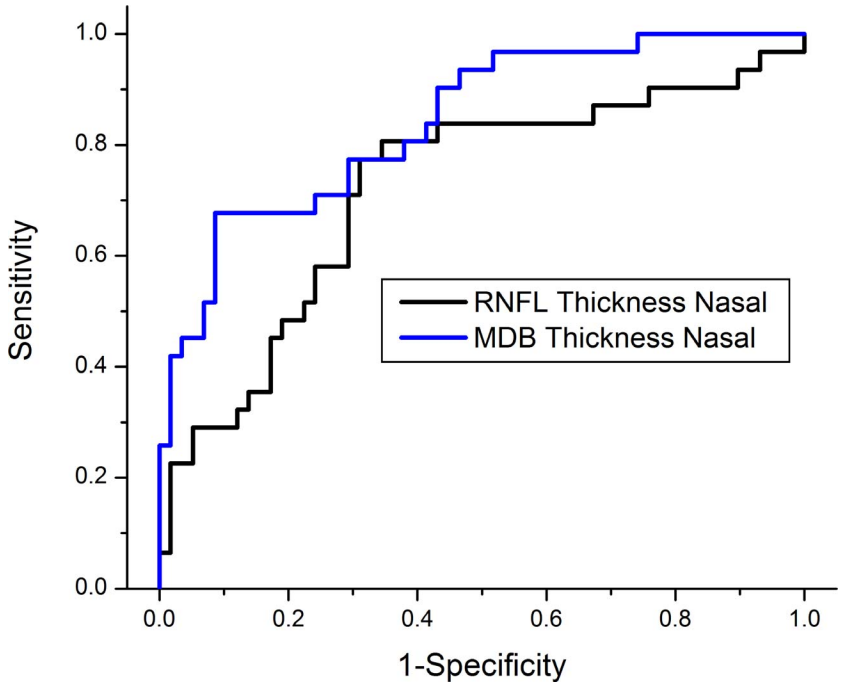

Figure 6. The ROC curve of the RNFL thickness compared with the ROC curve for MDB thickness in the nasal quadrant. The difference in the AUROC curves (MDB AUROC = 0.913, RNFL thickness AUROC = 0.818, $P = 0.004$) was statistically significant.

Table 3. Comparison of Diagnostic Capabilities for Glaucoma of the RNFL Thickness Versus Five Neuroretinal Rim Parameters: The MDB Thickness, MDB Area, Rim Volume, Rim Area, and Rim Thickness

Region	MDB Thickness AUROC	RNFL Thickness AUROC	*P* Value
Global	0.968	0.954	0.260
Inferior	0.966	0.958	0.428
Superior	0.953	0.936	0.260
Nasal	0.913	0.818	0.004
Temporal	0.922	0.858	0.026
IT	0.968	0.958	0.392
IN	0.950	0.897	0.011
ST	0.960	0.931	0.066
SN	0.933	0.868	0.012
Region	**MDB Area AUROC**	**RNFL Thickness AUROC**	***P* Value**
Global	0.969	0.954	0.230
Inferior	0.952	0.958	0.614
Superior	0.941	0.936	0.776
Nasal	0.886	0.818	0.055
Temporal	0.894	0.858	0.272
IT	0.955	0.958	0.827
IN	0.924	0.897	0.212
ST	0.939	0.931	0.671
SN	0.886	0.868	0.528
Region	**Rim Volume AUROC**	**RNFL Thickness AUROC**	***P* Value**
Global	0.952	0.954	0.912
Inferior	0.950	0.958	0.563
Superior	0.932	0.936	0.842
Nasal	0.895	0.818	0.025
Temporal	0.909	0.858	0.093
IT	0.949	0.958	0.522
IN	0.934	0.897	0.084
ST	0.939	0.931	0.651
SN	0.909	0.868	0.152
Region	**Rim Area AUROC**	**RNFL Thickness AUROC**	***P* Value**
Global	0.908	0.954	0.029
Inferior	0.897	0.958	0.005
Superior	0.890	0.936	0.068
Nasal	0.841	0.818	0.544
Temporal	0.843	0.858	0.688
IT	0.894	0.958	0.006
IN	0.865	0.897	0.241
ST	0.890	0.931	0.116
SN	0.853	0.868	0.634
Region	**Rim Thickness AUROC**	**RNFL Thickness AUROC**	***P* Value**
Global	0.944	0.954	0.550
Inferior	0.952	0.958	0.645
Superior	0.919	0.936	0.354
Nasal	0.878	0.818	0.096
Temporal	0.890	0.858	0.317
IT	0.943	0.958	0.318
IN	0.937	0.897	0.069
ST	0.931	0.931	0.973
SN	0.890	0.868	0.460

AUROC, area under the receiver operating characteristic curve; IT, inferotemporal; IN, inferonasal; ST, superotemporal; SN, supernonasal.

comparing the BMO-MRW to the RNFL thickness showed the largest differences in the nasal region. Our study showed that the nasal and temporal quadrants of the MDB thickness and the superonasal and inferonasal sectors of the MDB thickness had significantly higher AUROC values ($P = 0.004$–0.026) than the corresponding 2D RNFL regions. When evaluating Cirrus neuroretinal rim parameters, some studies using the Cirrus 200 A-line × 200 raster scan protocol have also suggested that rim thickness and area in the nasal and temporal quadrants have greater AUROC values compared with RNFL thickness values ($P < 0.001$)[35]; however, other Cirrus studies have suggested that there are no statistically significant differences between the 2D rim thickness and area compared with the 2D RNFL thickness ($P > 0.05$).[11] Even though glaucoma preferentially causes superior and inferior thinning and even though these regions classically have the highest diagnostic capabilities, the nasal and temporal MDB thickness had higher AUROC values in 3D datasets compared with the 2D RNFL thickness. In the nasal region, the diagnostic capability of the RNFL thickness may be reduced by the high density of blood vessels. The RNFL is also typically thinnest in the temporal region, so the proportion of vascular and glial tissue is higher, making the temporal RNFL thickness less sensitive to change (floor effect). The nasal and temporal MDB thickness measurements may be able to detect pathological change more easily because of the higher proportion of nerve tissue at the neuroretinal rim. Hwang and Kim[35] also suggested that differences in the topographic distribution of RNFL and rim loss may be a cause of the differences in diagnostic abilities between the RNFL thickness and rim parameters in the nasal and temporal regions. In conclusion, of the BMO-MRW, MDB thickness, and Cirrus neuroretinal rim parameters, only the 3D MDB neuroretinal rim thickness and 2D Cirrus neuroretinal rim thickness and area had regions (i.e., nasally and temporally) that had significantly improved diagnostic capability compared with the 2D RNFL thickness, and both of these parameters were based on high-density raster scan protocols.

The Cirrus machine has many neuroretinal rim parameters in its software. None of them had significantly higher diagnostic capability than the RNFL thickness,[11,35,36] except for the nasal and temporal rim thickness and area.[35] The Cirrus optic nerve parameters are calculated from a 200 B-scan volume protocol, which is similar to the MDB 193 B-scan volume protocol. However, the Cirrus software (Cirrus software versions 5.0 and 6.0) calculates these parameters using a 200-μm reference plane above the RPE,[36] whereas the MDB does not use a reference surface. Mwanza et al.[11] noted that the following Cirrus optic nerve head parameters appear to have similar diagnostic ability as the 2D RNFL thickness: disc area, rim area, vertical rim thickness, horizontal rim thickness, cup-to-disc area ratio, vertical cup-to-disc ratio, horizontal cup-to-disc ratio, and cup volume. Hwang and Kim[35] similarly showed that Cirrus neuroretinal rim assessments (rim area and rim thickness) were similar to the RNFL thickness in diagnostic capability for the global, superior, and inferior regions.

Although the MDB neuroretinal rim thickness has a significantly higher diagnostic capability than the RNFL thickness in the nasal and temporal quadrants, the diagnostic capability of the MDB area is not significantly higher than the RNFL thickness in any subfield. This finding is notable because the MDB area is calculated by using the same points as the MDB thickness (Fig. 2). Blood vessels and glial tissue may reduce the sensitivity of the area measurements quadratically, while affecting the neuroretinal rim thickness in only a linear fashion. Gardiner et al.[25] suggested this effect when comparing the BMO-MRW with the BMO minimum rim area. In addition to this floor effect, the reorientation of the blood vessels, as axonal tissue is lost in glaucoma, may reduce the sensitivity of

Investigative Ophthalmology & Visual Science

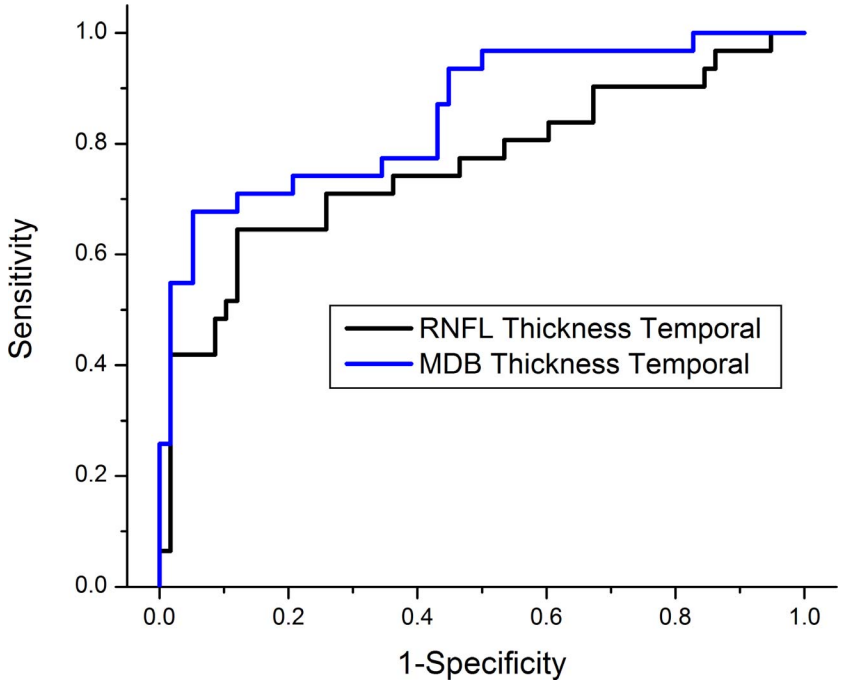

FIGURE 7. The ROC curve of the RNFL thickness compared with the ROC curve for the MDB thickness in the temporal quadrant. The difference in the AUROC curves (MDB AUROC = 0.922, RNFL thickness AUROC = 0.858, $P = 0.026$) was statistically significant.

both parameters but may affect the MDB area more. In contrast, the MDB area had a significantly higher diagnostic capability than the rim area in all but the nasal and superonasal fields. The rim area is a projection of the rim tissue volume on a horizontal plane, whereas the MDB area is a fully 3D measurement and may thus provide more information. Chauhan et al.[13] and Gardiner et al.[25] mention that the horizontal area measurements had lower diagnostic capability and structure-function correlation than the minimum rim width or area measurements.

The current study and the literature suggest that neuroretinal rim parameters (rim volume, area, and thickness), which are based on a 150-μm reference surface, have similar diagnostic capability to RNFL thickness (Table 3). On the Cirrus platform, which used a reference plane 200 μm above the RPE, Mwanza et al.[11] reported no statistically significant

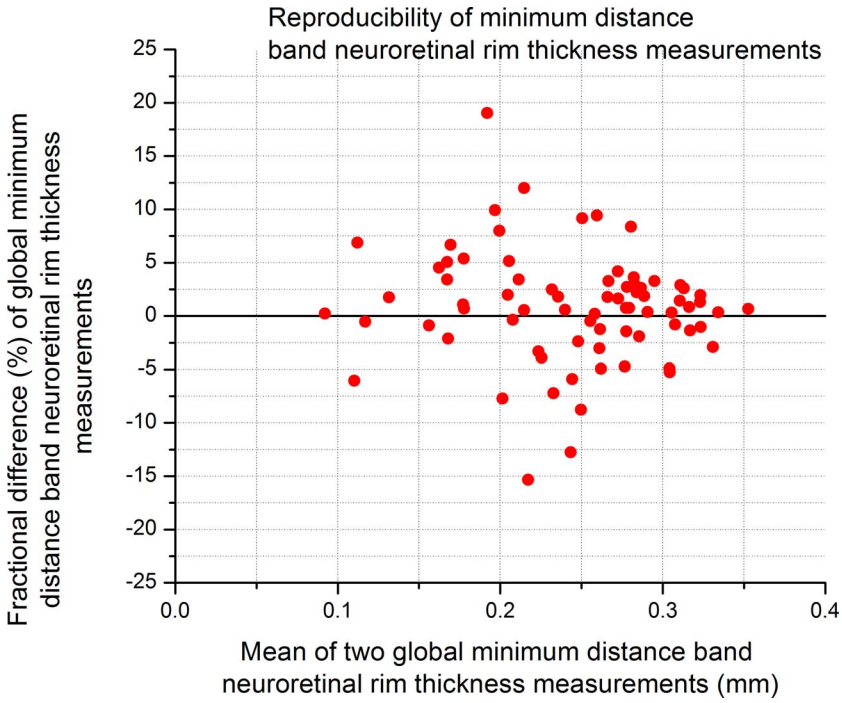

FIGURE 8. A Bland-Altman plot showing the reproducibility of the global MDB neuroretinal rim thickness. The intertest variability between two measurements (percentage fractional difference) is plotted against the mean of the measurements.

Investigative Ophthalmology & Visual Science

differences in AUROC for the top optic nerve parameters and the RNFL thickness measurements ($P > 0.05$). In the article by Hwang and Kim,[35] rim area and thickness had a higher diagnostic capability for the nasal and temporal quadrants, suggesting that the 200-μm reference plane may yield improved diagnostic performance compared with the 150-μm reference plane; however, a 200-μm reference plane may be higher than the level of the ILM in many patients, rendering neuroretinal rim parameters undefined in these cases.

The literature suggests that parameters calculated from high-density raster scan protocols over the optic nerve may have diagnostic capabilities the same as or higher than those derived from radial scan protocols over the same region. Pollet-Villard et al.[37] used the Cirrus platform with 36 radial sections generated from the 200 raster scans over the optic nerve to calculate the BMO-MRW. He reported that the BMO-MRW had a lower diagnostic capability than the RNFL thickness in that study (AUROC 0.906 vs. 0.922), and that the RNFL parameter with the highest AUROC (average RNFL) was statistically similar to the BMO-MRW parameter with the highest AUROC value (inferior temporal sector, $P > 0.1$). This Cirrus BMO-MRW parameter was calculated using manual identification of the disc margin in the radial scans. The report by Chauhan et al.[13] on the Spectralis BMO-MRW parameter suggests that the BMO-MRW has higher diagnostic capability than RNFL thickness. Both our study and Cirrus studies, which used 193 and 200 raster line scans, respectively, noted that the 3D MDB neuroretinal rim thickness and 2D Cirrus neuroretinal rim thickness and area had significantly higher diagnostic capability than the traditional 2D RNFL thickness parameter in the nasal and temporal regions (Table 3).[35]

The case-control design of this study may be a limitation of this work. In clinical practice, diagnostic tests are typically performed on glaucoma suspects,[38–40] not just on patients who have a confirmed diagnosis of glaucoma. If the SD-OCT parameters were calculated for a cohort of glaucoma suspects, reduced AUROC values may be observed. The direct comparison of the MDB and rim parameters with the current structural diagnostic standard, the RNFL thickness, mitigated this problem and allowed the relative parameter performances to be evaluated.

In conclusion, the 3D MDB neuroretinal rim thickness parameter, which is derived from high-density 3D volume scans, offers a high diagnostic capability for glaucoma and may be of significant clinical utility.

Acknowledgments

Funded by the Fidelity Charitable Fund (Harvard University), the Massachusetts Lions Eye Research Fund, an American Glaucoma Society Mid-Career Award, and National Institutes of Health UL 1 RR025758.

Disclosure: **E. Tsikata**, None; **R. Lee**, None; **E. Shieh**, None; **H. Simavli**, None; **C.J. Que**, None; **R. Guo**, None; **Z. Khoueir**, None; **J. de Boer**, Heidelberg Engineering (F), P; **T.C. Chen**, None

References

1. Tham Y-C, Li X, Wong TY, Quigley HA, Aung T, Cheng C-Y. Global prevalence of glaucoma and projections of glaucoma burden through 2040: a systematic review and meta-analysis. *Ophthalmology*. 2014;121:2081–2090.
2. Wu H, de Boer JF, Chen TC. Diagnostic capability of spectral-domain optical coherence tomography for glaucoma. *Am J Ophthalmol*. 2012;153:815–826.e2.
3. Kita Y, Kita R, Takeyama A, Takagi S, Nishimura C, Tomita G. Ability of optical coherence tomography-determined ganglion cell complex thickness to total retinal thickness ratio to diagnose glaucoma. *J Glaucoma*. 2013;22:757–762.
4. Sung KR, Na JH, Lee Y. Glaucoma diagnostic capabilities of optic nerve head parameters as determined by Cirrus HD optical coherence tomography. *J Glaucoma*. 2012;21:498–504.
5. van der Schoot J, Vermeer KA, de Boer JF, Lemij HG. The effect of glaucoma on the optical attenuation coefficient of the retinal nerve fiber layer in spectral domain optical coherence tomography images light attenuation in glaucomatous RNFL. *Invest Ophthalmol Vis Sci*. 2012;53:2424–2430.
6. Chen TC, Cense B, Pierce MC, et al. Spectral domain optical coherence tomography: ultra-high speed, ultra-high resolution ophthalmic imaging. *Arch Ophthalmol*. 2005;123:1715–1720.
7. Chen TC. Spectral domain optical coherence tomography in glaucoma: qualitative and quantitative analysis of the optic nerve head and retinal nerve fiber layer (an AOS thesis). *Trans Am Ophthalmol Soc*. 2009;107:254–281.
8. Povazay B, Hofer B, Hermann B, et al. Minimum distance mapping using three-dimensional optical coherence tomography for glaucoma diagnosis. *J Biomed Opt*. 2007;12:041204.
9. Staurenghi G, Sadda S, Chakravarthy U, Spaide RF, International Nomenclature for Optical Coherence Tomography (IN•OCT) Panel. Proposed lexicon for anatomic landmarks in normal posterior segment spectral-domain optical coherence tomography: the IN•OCT consensus. *Ophthalmology*. 2014;121:1572–1578.
10. Strouthidis NG, Yang H, Fortune B, Downs JC, Burgoyne CF. Detection of optic nerve head neural canal opening within histomorphometric and spectral domain optical coherence tomography data sets. *Invest Ophthalmol Vis Sci*. 2009;50:214–223.
11. Mwanza J-C, Oakley JD, Budenz DL, Anderson DR, Cirrus Optical Coherence Tomography Normative Database Study Group. Ability of cirrus HD-OCT optic nerve head parameters to discriminate normal from glaucomatous eyes. *Ophthalmology*. 2011;118:241–248.e1.
12. Yi K, Mujat M, Sun W, Park BH, de Boer JF, Chen TC. Peripapillary retinal thickness maps in the evaluation of glaucoma patients: a novel concept. *ISRN Ophthalmol*. 2011:146813.
13. Chauhan BC, O'Leary N, Almobarak FA, et al. Enhanced detection of open-angle glaucoma with an anatomically accurate optical coherence tomography-derived neuroretinal rim parameter. *Ophthalmology*. 2013;120:535–543.
14. He L, Yang H, Gardiner SK, et al. Longitudinal detection of optic nerve head changes by spectral domain optical coherence tomography in early experimental glaucoma. *Invest Ophthalmol Vis Sci*. 2014;55:574–586.
15. Strouthidis NG, Yang H, Reynaud JF, et al. Comparison of clinical and spectral domain optical coherence tomography optic disc margin anatomy. *Invest Ophthalmol Vis Sci*. 2009;50:4709–4718.
16. Drexler W, Fujimoto JG. State-of-the-art retinal optical coherence tomography. *Prog Retin Eye Res*. 2008;27:45–88.
17. Simavli H, Que CJ, Akduman M, et al. Diagnostic capability of peripapillary retinal thickness in glaucoma using 3D volume scans. *Am J Ophthalmol*. 2015;159:545–556.e2.
18. Wu H, de Boer JF, Chen TC. Reproducibility of retinal nerve fiber layer thickness measurements using spectral domain optical coherence tomography. *J Glaucoma*. 2011;20:470–476.
19. Alasil T, Wang K, Keane PA, et al. Analysis of normal retinal nerve fiber layer thickness by age, sex, and race using spectral domain optical coherence tomography. *J Glaucoma*. 2013;22:532–541.

20. Alasil T, Wang K, Yu F, et al. Correlation of retinal nerve fiber layer thickness and visual fields in glaucoma: a broken stick model. *Am J Ophthalmol*. 2014;157:953–959.
21. Field MG, Alasil T, Baniasadi N, et al. Facilitating glaucoma diagnosis with intereye retinal nerve fiber layer asymmetry using spectral-domain optical coherence tomography. *J Glaucoma*. 2016;25:167–176.
22. Liu Y, Simavli H, Que CJ, et al. Patient characteristics associated with artifacts in Spectralis optical coherence tomography imaging of the retinal nerve fiber layer in glaucoma. *Am J Ophthalmol*. 2015;159:565–576.e2.
23. Canny J. A computational approach to edge detection. *IEEE Trans Pattern Anal Mach Intell*. 1986;PAMI-8:679–698.
24. Otsu N. A threshold selection method from gray-level histograms. *Automatica*. 1975;11:285–296.
25. Gardiner SK, Ren R, Yang H, Fortune B, Burgoyne CF, Demirel S. A method to estimate the amount of neuroretinal rim tissue in glaucoma: comparison with current methods for measuring rim area. *Am J Ophthalmol*. 2014;157:540–549.e2.
26. Leung CK, Chan W-M, Hui Y-L, et al. Analysis of retinal nerve fiber layer and optic nerve head in glaucoma with different reference plane offsets, using optical coherence tomography. *Invest Ophthalmol Vis Sci*. 2005;46:891–899.
27. DeLong ER, DeLong DM, Clarke-Pearson DL. Comparing the areas under two or more correlated receiver operating characteristic curves: a nonparametric approach. *Biometrics*. 1988;44:837–845.
28. Minckler DS, McLean IW, Tso MO. Distribution of axonal and glial elements in the rhesus optic nerve head studied by electron microscopy. *Am J Ophthalmol*. 1976;82:179–187.
29. Mwanza J-C, Kim HY, Budenz DL, et al. Residual and dynamic range of retinal nerve fiber layer thickness in glaucoma: comparison of three OCT platforms. *Invest Ophthalmol Vis Sci*. 2015;56:6344–6351.
30. Danthurebandara VM, Vianna JR, Sharpe GP, et al. Diagnostic accuracy of glaucoma with sector-based and a new total profile-based analysis of neuroretinal rim and retinal nerve fiber layer thickness. *Invest Ophthalmol Vis Sci*. 2016;57:181–187.
31. Tun TA, Sun C-H, Baskaran M, et al. Determinants of optical coherence tomography-derived minimum neuroretinal rim width in a normal Chinese population. *Invest Ophthalmol Vis Sci*. 2015;56:3337–3344.
32. Almobarak FA, O'Leary N, Reis ASC, et al. Automated segmentation of optic nerve head structures with optical coherence tomography. *Invest Ophthalmol Vis Sci*. 2014;55:1161–1168.
33. El Chehab H, Delbarre M, Maréchal M, et al. New neuroretinal rim analysis with spectral domain optical coherence tomography, Spectralis (Heidelberg Engineering, Germany). Preliminary study. *J Fr Ophtalmol*. 2015;38:46–52.
34. Gardiner SK, Boey PY, Yang H, Fortune B, Burgoyne CF, Demirel S. Structural measurements for monitoring change in glaucoma: comparing retinal nerve fiber layer thickness with minimum rim width and area. *Invest Ophthalmol Vis Sci*. 2015;56:6886–6891.
35. Hwang YH, Kim YY. Glaucoma diagnostic ability of quadrant and clock-hour neuroretinal rim assessment using cirrus HD optical coherence tomography. *Invest Ophthalmol Vis Sci*. 2012;53:2226–2234.
36. Mwanza J-C, Chang RT, Budenz DL, et al. Reproducibility of peripapillary retinal nerve fiber layer thickness and optic nerve head parameters measured with cirrus HD-OCT in glaucomatous eyes. *Invest Ophthalmol Vis Sci*. 2010;51:5724–5730.
37. Pollet-Villard F, Chiquet C, Romanet J-P, Noel C, Aptel F. Structure-function relationships with spectral-domain optical coherence tomography retinal nerve fiber layer and optic nerve head measurements. *Invest Ophthalmol Vis Sci*. 2014;55:2953–2962.
38. Medeiros FA, Ng D, Zangwill LM, et al. The effects of study design and spectrum bias on the evaluation of diagnostic accuracy of confocal scanning laser ophthalmoscopy in glaucoma. *Invest Ophthalmol Vis Sci*. 2007;48:214–222.
39. Lijmer JG, Mol BW, Heisterkamp S, et al. Empirical evidence of design-related bias in studies of diagnostic tests. *JAMA*. 1999;282:1061–1066.
40. Li T, Jampel HD. Imaging the posterior pole in glaucoma: necessary but not sufficient. *Ophthalmology*. 2016;123:926–927.